

High-order and Mass-conservative Regularized Implicit-explicit relaxation Runge-Kutta methods for the logarithmic Schrödinger equation

Jingye Yan¹, Hong Zhang², Yabing Wei^{3*}, Xu Qian²

¹ College of Mathematics and Physics, Wenzhou University, Wenzhou 325035, China

² Department of Mathematics, National University of Defense Technology, Changsha 410073, China

³ School of Mathematical Sciences, Jiangsu University, Zhenjiang 212013, China

Abstract

The non-differentiability of the singular nonlinearity (such as $f = \ln |u|^2$) at $u = 0$ presents significant challenges in devising accurate and efficient numerical schemes for the logarithmic Schrödinger equation (LogSE). To address this singularity, we propose an energy regularization technique for the LogSE. For the regularized model, we utilize Implicit-Explicit Relaxation Runge-Kutta methods, which are linearly implicit, high-order, and mass-conserving for temporal discretization, in conjunction with the Fourier pseudo-spectral method in space. Ultimately, numerical results are presented to validate the efficiency of the proposed methods.

Keywords: Logarithmic Schrödinger equation; non-differentiability; linear implicit; mass conservation; high order

1. Introduction

In this paper, we focus on the numerical solution for the logarithmic Schrödinger equation (LogSE), which take the form:

$$\begin{cases} i\partial_t u(\mathbf{x}, t) + \Delta u(\mathbf{x}, t) = \lambda u f(u), & \mathbf{x} \in \Omega, \quad t > 0, \\ u(\mathbf{x}, 0) = u_0(\mathbf{x}), & \mathbf{x} \in \bar{\Omega}, \end{cases} \quad (1.1)$$

where $i = \sqrt{-1}$, $f(u) = \ln(|u(\mathbf{x}, t)|^2)$, $\Omega \subset \mathbb{R}^d$, with $d \geq 1$, represents a bounded domain with a smooth boundary. The function u_0 is a given initial condition with a regularity that will be specified later. The constant $\lambda \neq 0$ is a real number, where for $\lambda > 0$, the solution exhibits repulsive or defocusing behavior, and for $\lambda < 0$, the solutions demonstrate attractive or focusing interactions. The LogSE (1.1) proposed as a model for nonlinear wave mechanics [4].

LogSE (1.1) conserves both mass and energy as follows,

$$\begin{aligned} M(t) &:= \int_{\Omega} |u(\mathbf{x}, t)|^2 d\mathbf{x} \equiv \int_{\Omega} |u_0(\mathbf{x})|^2 d\mathbf{x} = M(0), \\ E(t) &:= \int_{\Omega} [|\nabla u(\mathbf{x}, t)|^2 d\mathbf{x} + \lambda F(|u(\mathbf{x}, t)|^2)] d\mathbf{x} \\ &\equiv \int_{\Omega} [|\nabla u_0(\mathbf{x})|^2 + \lambda F(|u_0(\mathbf{x})|^2)] d\mathbf{x} = E(0), \end{aligned} \quad (1.2)$$

¹*Corresponding author.

E-mail address: weiyb@buaa.edu.cn (Y. Wei)

where

$$F(\rho) = \int_0^\rho \ln(s) ds = \rho \ln \rho - \rho, \quad \rho = |u|^2. \quad (1.3)$$

The nonlinearity term $f(u) = \ln(|u(x, t)|^2)$ is non-differentiable at $u = 0$. This characteristic introduces significant practical challenges and theoretical complexities, particularly when it comes to analyzing and solving the numerical solutions of the LogSE (1.1). Consequently, the existing literature on this topic is somewhat limited. For the Cauchy problem associated with the LogSE, Cazenave [6] established a suitable functional framework.

Extensive literature exists on numerical solutions for the Schrödinger equation with smooth nonlinearity, employing methods such as the finite difference method [2], time-splitting method [3, 1], and among others. However, for the LogSE (1.1), the available numerical schemes are more limited. This scarcity arises because these methods cannot be directly applied to the LogSE due to the non-differentiability of the nonlinearity at $u = 0$. To circumvent this issue, Bao [2, 1] introduced a regularized logarithmic Schrödinger equation by substituting $f(u)$ with $f_\varepsilon(u^\varepsilon)$, where $0 < \varepsilon \ll 1$. They developed a semi-implicit finite difference method [2], which, although not conserving energy, provided a viable approach. Later, Bao [3] introduced a different regularization strategy at the energy density level, substituting the energy density locally in the region $0 < \rho < \varepsilon^2$ with a sequence of polynomials while keeping it unchanged in the region $\rho \geq \varepsilon^2$. In [3, 1], Bao constructed regularized Lie-Trotter splitting and Strang splitting methods, which preserve mass conservation but are only first and second order, respectively, for solving the LogSE. Recently, Wang [11] developed a nonregularized first-order implicit-explicit scheme for the LogSE, with the nonlinearity being explicit but only first order in time.

Over the past decades, a variety of relaxation Runge-Kutta (RRK) methods [9] have been developed, offering explicit and mass conservative solutions. However, these explicit methods are plagued by stringent step size restrictions that can limit their practical applicability. Recently, Li [10] investigated implicit-explicit relaxation Runge-Kutta (IMEX RRK) methods for nonlinear stiff ordinary differential equations. The proposed methods are linearly implicit, can achieve arbitrarily high order accuracy, and are designed to preserve monotonicity.

The structure of the rest of this paper is as follows: Section 2 introduces the energy regularized logarithmic Schrödinger equation (ERLogSE). In Section 3, IMEX RRK methods are applied to discretize the ERLogSE in time, combined with the Fourier pseudo-spectral method for spatial discretization. Section 4 presents several numerical experiments to demonstrate the efficiency and accuracy of the proposed numerical methods. Finally, Section 6 concludes the paper.

2. The energy regularized LogSE

In this context, the energy-regularization technique proposed by Bao et al. in [3] is employed to address the singularity issue of the logarithmic term in the LogSE. This approach uses a polynomial approximation to smooth out the singularity at the origin for the energy density function $F(\rho)$, as depicted in equation (1.3). The energy regularized method, as demonstrated in [3], yields superior performance compared to direct regularization of the logarithmic nonlinearity in the LogSE. The energy density $F(\rho)$ is approximated using a piecewise smooth function that incorporates a polynomial approximation near the origin as follows,

$$F_k^\varepsilon(\rho) = F(\rho)\chi_{\{\rho \geq \varepsilon^2\}} + P_{k+1}^\varepsilon(\rho)\chi_{\{\rho < \varepsilon^2\}}, \quad k \geq 2, \quad (2.1)$$

where χ_A is the characteristic function of the set A and

$$P_{k+1}^\varepsilon(\rho) = \rho \ln \varepsilon^2 - 1 - \sum_{j=1}^k \frac{1}{j} \left(1 - \frac{\rho}{\varepsilon^2}\right)^j$$

is a polynomial of degree $k + 1$, which allows $F_k^\varepsilon \in C^k([0, +\infty))$, $F_k^\varepsilon(0) = F(0) = 0$ (this satisfies the regularized energy to be well-defined on the whole space). We can obtain

$$\begin{aligned} f_k^\varepsilon(\rho) &= (F_k^\varepsilon)'(\rho) = \ln \rho \chi_{\{\rho \geq \varepsilon^2\}} + (P_{k+1}^\varepsilon)'(\rho) \chi_{\{\rho < \varepsilon^2\}} \\ &= \ln \rho \chi_{\{\rho \geq \varepsilon^2\}} + \left[\ln(\varepsilon^2) - \frac{k+1}{k} \left(1 - \frac{\rho}{\varepsilon^2}\right)^k - \sum_{j=1}^{k-1} \frac{1}{j} \left(1 - \frac{\rho}{\varepsilon^2}\right)^j \right] \chi_{\{\rho < \varepsilon^2\}}, \quad \rho \geq 0. \end{aligned} \quad (2.2)$$

One can get the energy regularized logarithmic Schrödinger equation (ERLogSE) with a small parameter $0 < \varepsilon \ll 1$ as follows

$$\begin{cases} i\partial_t u^\varepsilon(\mathbf{x}, t) + \Delta u^\varepsilon(\mathbf{x}, t) = \lambda u^\varepsilon f_\varepsilon^k(u^\varepsilon), & \mathbf{x} \in \Omega, \quad t > 0, \\ u^\varepsilon(\mathbf{x}, 0) = u_0(\mathbf{x}), & \mathbf{x} \in \bar{\Omega}, \end{cases} \quad (2.3)$$

which preserves the mass conservation law

$$M^\varepsilon(t) := \int_{\Omega} |u^\varepsilon(\mathbf{x}, t)|^2 d\mathbf{x} \equiv \int_{\Omega} |u_0(\mathbf{x})|^2 d\mathbf{x} = M(0), \quad (2.4)$$

where f_ε^k defined in (2.2) for ERLogSE.

3. The construction of Regularized IMEX RRK methods

3.1. High order Regularized IMEX RRK methods

We rewrite ERLogSE (2.3) as

$$u_t^\varepsilon = g^I(u^\varepsilon) + g^E(u^\varepsilon), \quad (3.1)$$

where $g^I(u^\varepsilon) = i\Delta u^\varepsilon$, $g^E(u^\varepsilon) = i\lambda u^\varepsilon f_\varepsilon^k(u^\varepsilon)$.

Applying the different orders IMEX RRK methods to the ERLogSE (3.1). We can get the semi-discrete system as follows:

$$\begin{cases} u_i^\varepsilon = u_\gamma^{\varepsilon, n} + \tau \sum_{j=1}^i a_{ij}^I g_j^I + \tau \sum_{j=1}^{i-1} a_{ij}^E g_j^E, & i = 1, \dots, s, \\ u_\gamma^{\varepsilon, n+1} = u_\gamma^{\varepsilon, n} + \tau \gamma_n \sum_{j=1}^s b_j^I g_j^I + \tau \gamma_n \sum_{j=1}^s b_j^E g_j^E, \end{cases} \quad (3.2)$$

where $g_j^I = g^I(t_n + c_j \tau, u_j^\varepsilon)$, $g_j^E = g^E(t_n + c_j \tau, u_j^\varepsilon)$, $j = 1, \dots, s$, and $u_\gamma^{\varepsilon, n+1}$ is the approximation at $\hat{t}_{n+1} = \hat{t}_n + \gamma_n \tau$. Define

$$\begin{aligned} A^I &= (a_{ij}^I)_{s \times s}, \quad a_{ij}^I = 0 \text{ for } j > i, \\ A^E &= (a_{ij}^E)_{s \times s}, \quad a_{ij}^E = 0 \text{ for } j \geq i, \\ b^I &= (b_1^I, \dots, b_s^I)^T, \quad b^E = (b_1^E, \dots, b_s^E)^T, \end{aligned}$$

and the s-stage IMEX RK method can be represented by a double Butcher tableau,

$$\begin{array}{c|c} c^I & A^I \\ \hline & (b^I)^T \end{array}, \quad \begin{array}{c|c} c^E & A^E \\ \hline & (b^E)^T \end{array},$$

where $c_i^I = \sum_{j=1}^s a_{ij}^I$, $c_i^E = \sum_{j=1}^s a_{ij}^E$, $i = 1, \dots, s$.

We rewrite (3.2) into

$$\begin{cases} u_i^\varepsilon = u_\gamma^{\varepsilon, n} + \tau \sum_{j=1}^i a_{ij}^I g_j^I + \tau \sum_{j=1}^{i-1} a_{ij}^E g_j^E, & i = 1, \dots, s, \\ u^{\varepsilon, n+1} = u_\gamma^{\varepsilon, n} + \tau \sum_{j=1}^s b_j^I g_j^I + \tau \sum_{j=1}^s b_j^E g_j^E, \\ u_\gamma^{\varepsilon, n+1} = u^{\varepsilon, n+1} + (\gamma_n - 1)(u^{\varepsilon, n+1} - u_\gamma^{\varepsilon, n}). \end{cases} \quad (3.3)$$

Theorem 3.1. For the semi-discrete scheme (3.2), if we set

$$\gamma_n = \begin{cases} 1, & \sum_{j=1}^s (b_j^I g_j^I + \tau \gamma_n \sum_{j=1}^s b_j^E g_j^E) = 0, \\ \frac{-2 \sum_{j=1}^s \Re(b_j^I g_j^I + b_j^E g_j^E, u_\gamma^{\varepsilon, n})}{\tau \|\sum_{j=1}^s b_j^I g_j^I + \sum_{j=1}^s b_j^E g_j^E\|^2}, & \sum_{j=1}^s (b_j^I g_j^I + \sum_{j=1}^s b_j^E g_j^E) \neq 0. \end{cases} \quad (3.4)$$

(3.2) would satisfy the conservation of mass:

$$\|u_\gamma^{\varepsilon,n+1}\|^2 = \|u_\gamma^{\varepsilon,n}\|^2. \quad (3.5)$$

Proof. From (3.2) and the definition of (3.4), we have

$$\begin{aligned} \|u_\gamma^{\varepsilon,n+1}\|^2 - \|u_\gamma^{\varepsilon,n}\|^2 &= \|u_\gamma^{\varepsilon,n} + \tau\gamma_n \sum_{j=1}^s b_j^I g_j^I + \tau\gamma_n \sum_{j=1}^s b_j^E g_j^E\|^2 - \|u_\gamma^{\varepsilon,n}\|^2 \\ &= \tau^2 \gamma_n^2 \left\| \sum_{j=1}^s b_j^I g_j^I + \sum_{j=1}^s b_j^E g_j^E \right\|^2 + 2\tau\gamma_n \sum_{j=1}^s \Re(b_j^I g_j^I + b_j^E g_j^E, u_\gamma^{\varepsilon,n}) \\ &= 0. \end{aligned} \quad (3.6)$$

This ends the proof. \square

Lemma 3.1. [10] Suppose that the given IMEX RK method is p -th order accurate with $p \geq 2$. For sufficiently small τ , the relaxation coefficient γ_n defined in (3.4) satisfies

$$\gamma_n = 1 + O(\tau^{p-1}). \quad (3.7)$$

Theorem 3.2. The truncation error of IMEX RRK method (3.3) is $O(\tau^{p+1})$.

Proof. Since the convergence order of IMEX RK method is $O(\tau^p)$, putting the exact solution into the second equation of (3.3), one can obtain

$$u^\varepsilon(\hat{t}_n + \tau) = \Phi_n(u^\varepsilon(t)) + O(\tau^{p+1}),$$

where

$$\Phi_n(u^\varepsilon(t)) = u^\varepsilon(\hat{t}_n) + \tau \sum_{j=1}^s b_j^I g_j^I(u^\varepsilon(\hat{t}_{nj})) + \tau \sum_{j=1}^s b_j^E g_j^E(u^\varepsilon(\hat{t}_{nj})),$$

and $\hat{t}_{nj} = \hat{t}_n + c_j \tau$, $j = 1, \dots, s$.

Then substitute the exact solution into the third equation of (3.3), we obtain the truncation error of the third equation of (3.3) as follows

$$\begin{aligned} \mathcal{T}^{n+1} &= u^\varepsilon(\hat{t}_{n+1}) - \Phi_n(u^\varepsilon(t)) - (\gamma_n - 1)(\Phi_n(u^\varepsilon(t)) - u^\varepsilon(\hat{t}_n)) \\ &= u^\varepsilon(\hat{t}_{n+1}) - (u^\varepsilon(\hat{t}_n + \tau) + O(\tau^{p+1})) - (\gamma_n - 1)(u^\varepsilon(\hat{t}_n + \tau) + O(\tau^{p+1}) - u^\varepsilon(\hat{t}_n)) \\ &= u^\varepsilon(\hat{t}_{n+1}) - u^\varepsilon(\hat{t}_n + \tau) - (\gamma_n - 1)(u^\varepsilon(\hat{t}_n + \tau) - u^\varepsilon(\hat{t}_n)) + O(\tau^{p+1}) + O((\gamma_n - 1)\tau^{p+1}) \\ &= u^\varepsilon(\hat{t}_n + \tau + (\gamma_n - 1)\tau) - u^\varepsilon(\hat{t}_n + \tau) - (\gamma_n - 1)u^{\varepsilon'}(\hat{t}_n + \tau)\tau + O(\tau^{p+1}) \\ &= u^\varepsilon(\hat{t}_n + \tau) + (\gamma_n - 1)\tau u^{\varepsilon'}(\hat{t}_n + \tau) + O((\gamma_n - 1)^2 \tau^2) \\ &\quad - u(\hat{t}_n + \tau) - (\gamma_n - 1)\tau u^{\varepsilon'}(\hat{t}_n + \tau) + O(\tau^{p+1}) = O(\tau^{p+1}), \end{aligned}$$

where we used $\hat{t}_{n+1} = \hat{t}_n + \gamma_n \tau$. This ends the proof. \square

4. Numerical Experiments

In the numerical test, the following RK methods will be used in time:

1. RK(1,2), Implicit-explicit midpoint [7];
2. RK(2,3), two-stage, third-order RK [7];
3. RK(6,4), also named ARK4(3)6L[2]SA in [8];
4. RK(8,5), also named ARK5(4)8L[2]SA in [8],

and we apply Fourier pseudo-spectral method in space where can be used FFT method. We only show numerical results for the ERLogSE, the results of ERSSE are quite similar which are omitted for brevity.

4.1. Accuracy test

Consider the LogSE (1.1) with the exact Gaussian solution [5] in 1-dimension as follows,

$$u(x, t) = b \exp(i(x \cdot \zeta - (a + |\zeta|^2)t) + (\lambda/2)|x - 2\zeta t|^2), \quad x \in \mathbb{R}, \quad t \geq 0, \quad (4.1)$$

where $a = -\lambda(1 - \ln|b|^2)$, $b \in \mathbb{R}$ and $\lambda, \zeta \in \mathbb{R}$ are given constants. To quantify the numerical errors, we define the following error functions:

$$\begin{aligned} e^\varepsilon(t_n) &= u_{ref}^\varepsilon(\cdot, t_n) - u^{\varepsilon, n}, & \hat{e}^\varepsilon(t_n) &= u_{ex}(\cdot, t_n) - u_{ref}^\varepsilon(\cdot, t_n), \\ \hat{\rho}^\varepsilon(t_n) &= \rho_{ex}(\cdot, t_n) - \rho_{ref}^\varepsilon(\cdot, t_n) = |u_{ex}(\cdot, t_n)|^2 - |u_{ref}^\varepsilon(\cdot, t_n)|^2, & e_E^\varepsilon &= E(u_0) - E_k^\varepsilon(u_0). \end{aligned} \quad (4.2)$$

Here $u_j^{\varepsilon, n}$ is the numerical solution, u_{ex} is the exact solution of LogSE (1.1), u_{ref}^ε is the ‘exact’ solution of ERLogSE (2.3) with $h_e = \frac{5}{2\pi}$, $\tau_e = 10^{-5}$. The initial data is taken as $u_0 = u(x, 0)$ in (4.1) and the boundary conditions are given such that the exact solution. Here $\zeta = 0$, $T = 1$, $\Omega = [-10, 10]$, $\lambda = -1$, $b = 1$.

4.1.1. Convergence rate of the regularized model

Here we consider the error between the solutions of the ERLogSE (2.3) and the LogSE (1.1). Fig. 4.1 depicts $\|\hat{e}^\varepsilon\|$, $\|\hat{\rho}^\varepsilon\|$, e_E^ε at $t = 1$ with different regularized nonlinearities f_2^ε , f_{10}^ε computed by IMEX RRK(2,3), and other RRK schemes are not depicted here for the sake of conciseness. We can draw the following conclusions: (i) The solution of ERLogSE (2.3) converges linearly to LogSE (1.1) in terms of ε ; (ii) The density ρ^ε of the solution of ERLogSE (2.3) exhibits linear convergence to that of the LogSE (1.1) in terms of ε ; (iii) The regularized energy E_k^ε converges quadratically to the original energy E ; (iv) Across these three figures, it is evident that for any given ε , the solutions with larger values of n yield superior performance.

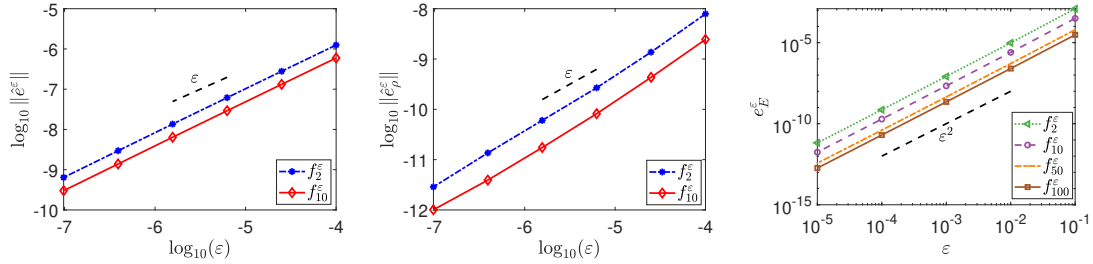


Fig. 4.1. Convergence order ERLogSE to LogSE, i.e. $\|\hat{e}^\varepsilon(t = 1)\|$, $\|\hat{\rho}^\varepsilon(t = 1)\|$, $e_E^\varepsilon(t = 1)$.

4.1.2. Convergence rate of the numerical scheme

Firstly, we investigate the relaxation coefficient γ_n at $t = 1$ for various values of n , ε and the results shown in Fig.4.2, substantiate Lemma 3.1.

Next, to assess the temporal convergence rate, we set the mesh size to $h = h_e$, and varied the time step as $\tau = 2^{-j} \times 10^{-1}$ for $j = 1, 2, \dots, 5$ with $n = 2$, $n = 4$ under different ε . Fig.4.3 displays the temporal convergence rates of the IMEX RRK methods, calculated using various schemes. The RRK methods show a convergence rate of p , confirming the theoretical predictions in Theorem 3.2.

Additionally, to evaluate the spatial convergence rate of the Fourier pseudo-spectral method, we fixed the time step $\tau = \tau_e$, and $\varepsilon = 10^{-6}$ and selected different numbers of grid points $N_j = 8 + 2(j + 1)$, $j = 1, 2, \dots, 5$. Table 4.1 illustrates the spatial convergence rates of the IMEX RRK method, with the RRK(2,3) scheme being particularly noteworthy.

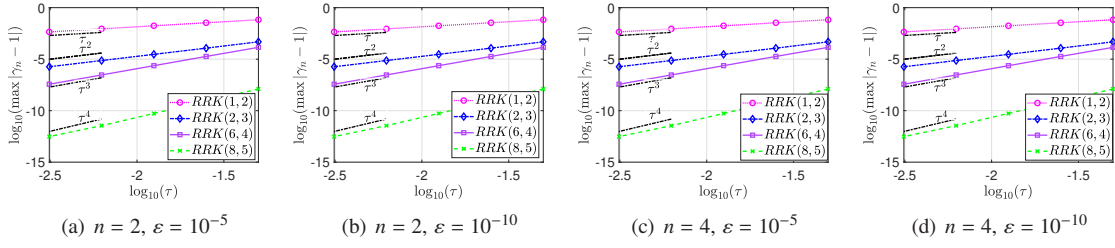


Fig. 4.2. Convergence order of $\max(|\gamma_n - 1|)$ for different IMEX RRK schemes.

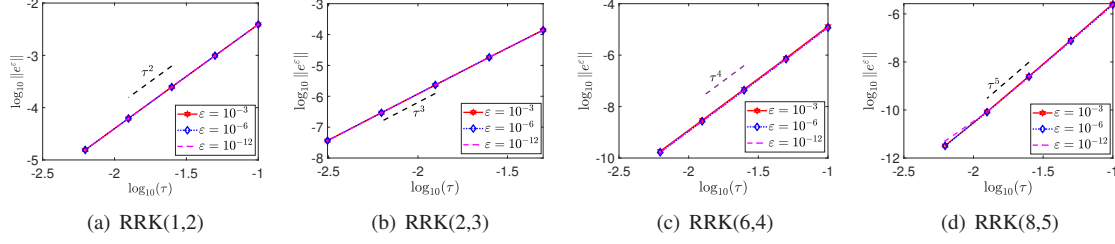


Fig. 4.3. Convergence order in time of RRK with different ϵ .

4.2. Dynamics

In this section, we investigate long time dynamics of LogSE with Gaussian-type initial datum in 1D. To this end, we fix $\lambda = -1$, $x \in [-40, 40]$, $\tau = 2 \times 10^{-3}$, $h = \frac{5}{16}$. The initial datum is chosen as

$$u_0(x) = \sum_{k=1}^2 b_k e^{-\frac{a_k}{2}(x-x_k)^2 + i v_k x}, \quad x \in \mathbb{R}, \quad (4.3)$$

where b_k , a_k , x_k and v_k are real constants, i.e, the initial data is the sum of 2 Gaussons with velocity v_k and initial location x_k . We take $v_1 = -v_2 = 2$, $x_1 = -x_2 = -30$, $b_k = a_k = 1$ ($k = 1, 2$).

Analyzing Fig. 4.4, we observe the following behaviors: (i) The mass is well conserved throughout the simulations, indicating the effectiveness of our numerical methods in preserving this fundamental property; (ii) In the case of moving Gaussons, they pass completely through each other, eventually moving separately. Oscillations occur during the interaction.

5. Conclusion

We introduced an energy regularization approach to address the singularity present in the LogSE (1.1) by employing a polynomial approximation. Subsequently, we developed a family of IMEX RRK methods, combined

Table 4.1: Space accuracy tests of the Fourier spectral discretization ($\tau = 1 \times 10^{-5}$, $\epsilon = 10^{-6}$, $T = 1$).

RK (Stage, Order)	N	RRK	
		e^ϵ	order
(2,3)	12	2.54e-01	-
	14	1.38e-01	3.95
	16	5.59e-02	6.77
	18	1.66e-02	10.30
	20	3.73e-03	14.17

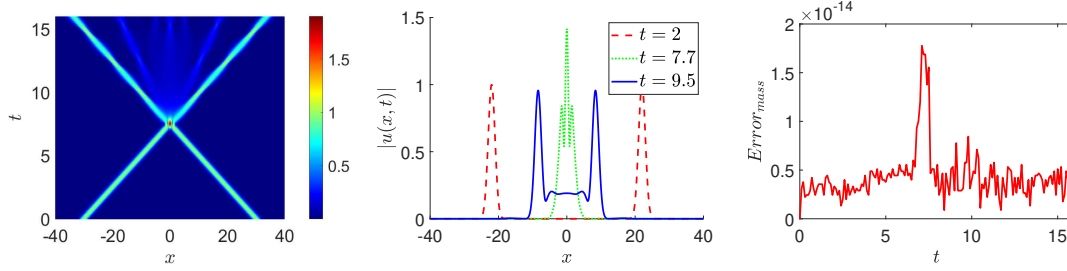


Fig. 4.4. Plots of $|u^E(x, t)|$ (first column); $|u^E(x, t)|$ at different time (second column) and evolution of mass error (third column) (Case for RRK(2,3)).

with the Fourier spectral method, to solve the ERLogSE (2.3). Our analysis demonstrated that these IMEX RRK methods not only inherit the mass conservation properties but also maintain the same convergence order as their standard counterparts. Furthermore, we conducted numerical experiments that substantiated our theoretical findings

Acknowledgements

The work is supported by the National Natural Science Foundation of China (No. 12271523), Natural Science Foundation of Zhejiang Province (No. Q24A010031), Scientific Research Fund of Zhejiang Provincial Education Department (No. Y202352579), Natural Science Foundation of Jiangsu Province, (No. BK20240832), Defense Science Foundation of China (No. 2021-JCJQ-JJ-0538), Science & Technology Innovation Program of Hunan Province (No. 2022RC1192).

References

References

- [1] W.Z. Bao, R. Carles, C.M. Su, and Q.L. Tang. Error estimates of a regularized finite difference method for the logarithmic Schrödinger equation. *SIAM J. Numer. Anal.*, 57(2):657–680, 2019.
- [2] W.Z. Bao, R. Carles, C.M. Su, and Q.L. Tang. Regularized numerical methods for the logarithmic Schrödinger equation. *Numer. Math.*, 143(2):461–487, 2019.
- [3] W.Z. Bao, R. Carles, C.M. Su, and Q.L. Tang. Error estimates of local energy regularization for the logarithmic Schrödinger equation. *Math. Models Methods Appl. Sci.*, 32(1):101–136, 2022.
- [4] I. Białynicki-Birula and J. Mycielski. Nonlinear wave mechanics. *Ann. Physics*, 100(1-2):62–93, 1976.
- [5] R. Carles and I. Gallagher. Universal dynamics for the defocusing logarithmic Schrödinger equation. *Duke Math. J.*, 167(9):1761–1801, 2018.
- [6] T. Cazenave and A. Haraux. *évolution equations with logarithmic nonlinearity. Annales of the Faculty of Sciences of Toulouse: Mathématique*, 5th série, 2(1):21–51, 1980.
- [7] M. Herty, L. Pareschi, and S. Steffensen. Implicit-explicit Runge-Kutta schemes for numerical discretization of optimal control problems. *SIAM J. Numer. Anal.*, 51(4):1875–1899, 2013.
- [8] C. A. Kennedy and M. H. Carpenter. Additive Runge-Kutta schemes for convection-diffusion-reaction equations. *Appl. Numer. Math.*, 44(1-2):139–181, 2003.
- [9] D.I. Ketcheson. Relaxation Runge-Kutta methods: conservation and stability for inner-product norms. *SIAM J. Numer. Anal.*, 57(6):2850–2870, 2019.
- [10] D.F. Li, X.X. Li, and Z.M. Zhang. Implicit-explicit relaxation Runge-Kutta methods: construction, analysis and applications to PDEs. *Math. Comp.*, 92(339):117–146, 2023.
- [11] Li-Lian Wang, J.Y. Yan, and X.L. Zhang. Error analysis of a first-order IMEX scheme for the logarithmic Schrödinger equation. *SIAM J. Numer. Anal.*, 62(1):119–137, 2024.